Wave-packet scattering at a normal-superconductor interface in two-dimensional materials : a generalized theoretical approach

Reference:
Linard F.J.A., Moura V.N., Covaci Lucian, Milošević Milorad, Chaves Andrey.- Wave-packet scattering at a normal-superconductor interface in two-dimensional materials : a generalized theoretical approach
Physical review B / American Physical Society - ISSN 2469-9969 - 107:16(2023), 165306
Full text (Publisher's DOI): https://doi.org/10.1103/PHYSREVB.107.165306
To cite this reference: https://hdl.handle.net/10067/1967090151162165141

Wave-packet scattering at a normal-superconductor interface in two-dimensional materials: a generalized theoretical approach

F. J. A. Linard,[1] V. N. Moura,[1] L. Covaci,[2] M. V. Milošević,[2] and A. Chaves[1,2,*]

[1]*Departamento de Física, Universidade Federal do Ceará, Caixa Postal 6030, 60455-760 Fortaleza, Ceará, Brazil*

[2]*Department of Physics, University of Antwerp, Groenenborgerlaan 171, B-2020, Antwerpen, Belgium*

A wave-packet time evolution method, based on the split-operator technique, is developed to investigate the scattering of quasi-particles at a normal-superconductor interface of arbitrary profile and shape. As a practical application, we consider a system where low energy electrons can be described as Dirac particles, which is the case for most two-dimensional materials, such as graphene and transition metal dichalcogenides. However the method is easily adapted for other cases such as electrons in few layer black phosphorus, or any Schrödinger quasi-particles within the effective mass approximation in semiconductors. We employ the method to revisit Andreev reflection in mono, bi and trilayer graphene, where specular and retro reflection cases are observed for electrons scattered by a step-like superconducting region. The effect of opening a zero-gap channel across the superconducting region on the electron and hole scattering is also addressed, as an example of the versatility of the technique proposed here.

PACS numbers: 78.66.Db 71.70.Ej 71.35.-y

I. INTRODUCTION

It is widely known that electron states convert to holes after being reflected by a normal (N)/superconductor (SC) interface.[1] This effect, also known as Andreev reflection, exhibits peculiarities: if the incidence to the NS interface is normal, the electron is fully converted into a hole, whereas for oblique incidence, part of the wave function is reflected back to the normal region as an electron state. In a system consisting of a semiconductor material, with a considerable energy gap separating conduction and valence bands, the momentum of the hole, along with its energy dispersion, guarantees that the hole component of the wave function travels back in a trajectory that is parallel to that of the incident electron, which is then coined the term retro-reflection. However, it has been demonstrated that in monolayer graphene, where low energy electrons behave as massless Dirac fermions in a gapless band structure,[2] the energy dispersion is such that, for low Fermi levels, the hole component of the wave function travels back in the normal region in a trajectory that is parallel to that of the *reflected* electron, thus undergoing a *specular* Andreev reflection. This effect has been predicted by Beenakker in 2006[3] in a model for monolayer graphene, which was further extended to bilayer graphene,[4,5] and experimentally observed only recently.[5–8] A graphene-based device suggested by Bhandari et al.[9], where an applied magnetic field guides electrons from a N graphene region toward a SC one, has been recently employed as yet another way to probe Andreev reflection and electron-hole conversion at the N/SC interface, through the analysis of electron and hole cyclotron orbits as imaged by scanning gate microscopy. The multiple Andreev reflection processes experimentally observed in such a graphene-based N/SC interface under an applied magnetic field produces quantum Hall edge states, as demonstrated in Ref. [10].

Further suggestions have been made for experimental observation of Andreev scattering using N/SC interfaces based on different materials, such as transition metal dichalcogenides[11,12] and their heterostructures,[13] as well as on borophene.[14] A NS interface in monolayer black phosphorus[15] has also been recently theoretically proposed as a venue for the observation of Andreev reflection.[16] Since this is a ≈ 2 eV gap semiconductor,[17] only retro reflection is expected to occur, but many two-dimensional (2D) materials with zero gap exist[18–20] and may be suitable for the observation of specular Andreev reflection too. However, developing a different theory for each Hamiltonian describing each of the several classes of materials in the 2D materials family seems like an insurmountable challenge. Moreover, most of the techniques proposed in the literature for the study of Andreev scattering resort to plane waves-based methods which, although providing analytical solutions to the scattering problem, are harder to be adapted to physical situations involving arbitrary potentials and N/SC interface profiles, as well as in the presence of applied fields. This motivates us to develop a method that is easily adapted for any configuration of the potential and N/SC interface profiles, as well as for any form of the Hamiltonian describing the materials involved.

The time evolution of wave-packets scattering across N/SC/N interfaces in the context of three-dimensional (bulk) systems, with charge carriers following a parabolic dispersion (thus being described by a Schroedinger Hamiltonian), has been explored decades ago, in Ref. [21]. Later on, studies of supercurrents in SC/N/SC junctions,[22] as well as in ultrafast Josephson nanojunctions based on SC/device/SC interfaces with time-dependent Hamiltonians,[23] have also been developed using different approaches involving time-dependent Bogoliubov-de Gennes equation.

In this paper, we propose a generalized numerical tech-

nique to investigate wave-packet dynamics at N/SC interfaces with arbitrary profile. This technique is based on an extension of the so called split-operator method,[24,25] that accounts for the Bogoliubov-de Gennes Hamiltonian describing a superconductor and a Dirac-Weyl Hamiltonian describing the behavior of the charge carriers in the system. The method allows for the investigation of wave-packet scattering at the interface and the interplay between electron and hole states, allowing one to assume an arbitrary form for the interface and potential profiles and to conveniently change the system Hamiltonian for that of any 2D material. We apply the method to calculate transmission probabilities (i) in mono, bi, and tri-layer graphene-based N/SC interfaces, as well as (ii) in a system consisting of a monolayer graphene-based normal wave-guide defined by adjacent superconducting regions. The former demonstrates the versatility of the method proposed here, regarding its flexibility to be conveniently adapted to other system Hamiltonians for electrons in materials yet unexplored in the context of N/SC interfaces, while the results in the latter illustrate how the channel width and length can be used to tune the electron and hole components of the wave-packet that leaves the channel region.

II. WAVE-PACKET PROPAGATION METHOD

Consider a basis $(u_A\ u_B\ v_A\ v_B)^T$, where u_i and v_i ($i = A, B$) represent the i-th component of the 2-component spinor describing electrons and holes, respectively. The Bogoliubov-de Gennes (BdG) Hamiltonian[26] describing the NS interface is given by

$$H_{BdG} = \begin{pmatrix} H - E_F + U(\vec{r}) & \Delta(\vec{r}) \\ \Delta^*(\vec{r}) & -[H - E_F + U(\vec{r})] \end{pmatrix}, \quad (1)$$

where H is a 2×2 matrix Hamiltonian for charged particles in the material in its normal phase, $\Delta(\vec{r}) = \Delta_0(\vec{r})e^{i\phi}$ is a space-dependent superconducting gap, which is assumed to be non-zero only at the superconducting region, $U(\vec{r})$ is an external potential, and E_F is the Fermi level. Notice that each U, Δ, and E_F must be multiplied by a 2×2 identity matrix $\mathcal{I}$ (omitted here for the sake of convenience), so that H_{BdG} is a 4×4 matrix.

The time evolution of an arbitrary initial wave-packet

$$\Psi(\vec{r}, t = 0) = \begin{pmatrix} u_A \\ u_B \\ v_A \\ v_B \end{pmatrix} \times \psi(\vec{r}, 0), \quad (2)$$

is calculated as

$$|\Psi(\vec{r}, t + \Delta t)\rangle = e^{-i\frac{H_{BdG}}{\hbar}\Delta t}|\Psi(\vec{r}, t)\rangle. \quad (3)$$

The Hamiltonian H_{BdG} is conveniently split into parts that depend exclusively on real or reciprocal space coordinates

$$H_{BdG} = (H - E_F) \otimes \sigma_z + U(\vec{r}) \otimes \sigma_z + \Delta_0(\vec{r})(\cos\phi\mathcal{I} \otimes \sigma_x + \sin\phi\mathcal{I} \otimes \sigma_y), \quad (4)$$

where the first term retains only the terms that depend on reciprocal-space coordinates $\vec{k}$ and $\vec{\sigma}$ is the vector of Pauli matrices.

We perform the Suzuki-Trotter expansion[24,25,27] in the time evolution operator of Eq. (3), which allows us to apply the exponential of operators that involve $\vec{k}$ and $\vec{r}$ in a separate manner, see the Appendix for the full calculation. This approach will be demonstrated to be very convenient in the context of 2D materials, since low energy electrons in these systems are often described by 2×2 Dirac-Weyl Hamiltonians that can be re-written into the form $H = \vec{h} \cdot \vec{\sigma}$, provided one considers a proper $\vec{h}$. In this case, the exponentials involved in the time evolution operator are eventually re-written as a series of 4 × 4 matrices:

$$e^{-i\vec{W}_r \otimes \vec{\sigma}} = \mathcal{M}_r = \begin{pmatrix} A_- & 0 & B_- & 0 \\ 0 & A_- & 0 & B_- \\ B_+ & 0 & A_+ & 0 \\ 0 & B_+ & 0 & A_+ \end{pmatrix} \quad (5)$$

where $A_\pm = \cos\left(\frac{\Delta t}{2\hbar}\sqrt{\Delta_0^2 + U^2}\right) \pm i\sin\left(\frac{\Delta t}{2\hbar}\sqrt{\Delta_0^2 + U^2}\right)\frac{U}{\sqrt{\Delta_0^2+U^2}}$ and $B_\pm = -i\sin\left(\frac{\Delta t}{2\hbar}\sqrt{\Delta_0^2 + U^2}\right)\frac{\Delta_0 e^{\pm i\phi}}{\sqrt{\Delta_0^2+U^2}}$; and

$$e^{-i\vec{W}_k \otimes \vec{\sigma}} = \mathcal{M}_k = \begin{pmatrix} C_- & D_- & 0 & 0 \\ D_+ & C_+ & 0 & 0 \\ 0 & 0 & C'_- & D'_- \\ 0 & 0 & D'_+ & C'_+ \end{pmatrix}, \quad (6)$$

where $C_\pm = \left(\cos(\omega) \pm i\sin(\omega)\frac{\omega_z}{\omega}\right)e^{iE_F\frac{\Delta t}{\hbar}}$, $D_\pm = -i\sin(\omega)\frac{\omega_x \pm i\omega_y}{\omega}e^{iE_F\frac{\Delta t}{\hbar}}$, $C'_\pm = \left(\cos(\omega') \pm i\sin(\omega')\frac{\omega'_z}{\omega'}\right)e^{-iE_F\frac{\Delta t}{\hbar}}$, $D'_\pm = -i\sin(\omega')\frac{\omega'_x \pm i\omega'_y}{\omega'}e^{-iE_F\frac{\Delta t}{\hbar}}$, $\vec{\omega} = (h_x, h_y, h_z)\frac{\Delta t}{\hbar}$ and $\vec{\omega'} = (-h_x, -h_y, -h_z)\frac{\Delta t}{\hbar}$.

Thus, a wave-packet at an instant t, $|\Psi(\vec{r}, t)\rangle$, is propagated to $|\Psi(\vec{r}, t + \Delta t)\rangle$ as

$$|\Psi(\vec{r}, t + \Delta t)\rangle = \mathcal{M}_r\mathcal{M}_k\mathcal{M}_r|\Psi(\vec{r}, t)\rangle, \quad (7)$$

which is performed in three steps: (i) multiplying $|\Psi(\vec{r}, t)\rangle$ by $\mathcal{M}_r$, (ii) taking the Fourier transform of the resulting spinor and multiplying it by $\mathcal{M}_k$ in reciprocal space, and then (iii) taking the resulting spinor back to real space, by performing an inverse Fourier transform on it, and multiplying it by $\mathcal{M}_r$ again. The process is repeated until the propagation is performed for a given time interval. Notice that, since the matrix expansion in Eq. (14) is exact, the only error involved in this procedure is the $O(\Delta t^3)$ error resulting from the Suzuki-Trotter expansion in Eq. (13). As we consider a small time step $\Delta t = 0.1$ fs, this term can be neglected from now on.

Electron and hole probability densities are calculated

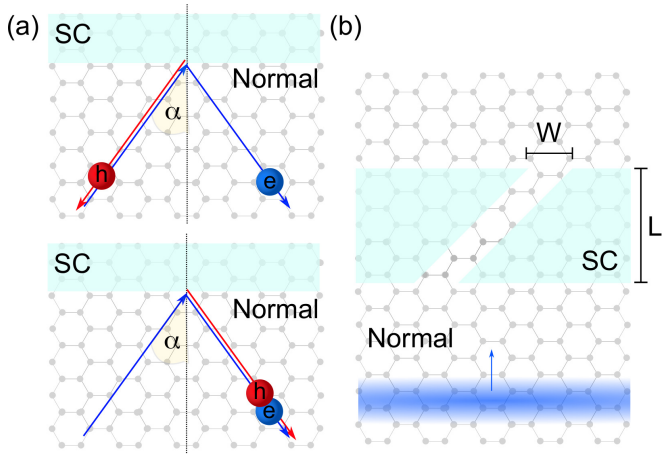

FIG. 1: (Color online) Sketch of the two graphene-based systems considered here: (a) a single interface between normal and superconducting (SC) regions, and (b) a tilted (by 45°) channel of length L and width W across the SC region. In the former, Andreev retro-(top) and specular (bottom) reflections will be investigated by calculating the trajectories of electron (e, blue) and holes (h, red), assuming an incidence angle α and describing the quasi-particles as circular gaussian wave-packets. As for the latter, we will investigate transmission/reflection probabilities for an incoming electron described by a gaussian wave front (blue gradient).

from the propagated electron-hole pseudo-spinor

$$\Psi(\vec{r},t) = \begin{pmatrix} \psi_{uA}(\vec{r},t) \\ \psi_{uB}(\vec{r},t) \\ \psi_{vA}(\vec{r},t) \\ \psi_{vB}(\vec{r},t) \end{pmatrix} \tag{8}$$

as

$$P_e(t) = \int_{r_1}^{r_2} [|\psi_{uA}(\vec{r},t)|^2 + |\psi_{uB}(\vec{r},t)|^2] d\vec{r} \tag{9}$$

$$P_h(t) = \int_{r_1}^{r_2} [|\psi_{vA}(\vec{r},t)|^2 + |\psi_{vB}(\vec{r},t)|^2] d\vec{r}, \tag{10}$$

where the interval $[r_1, r_2]$ limits the region of interest in space. For the systems shown in Fig. 1, the superconducting region covers the range $[-\infty, +\infty]$ in the horizontal x-axis [with the exception of the region inside the channel in Fig. 1(b)]. In the system in Fig. 1(a), the SC region goes from $y = 0$ to $y \to \infty$. In this case, as we are interested in the reflected quasi-particles in the N region, the integration region is taken as $[-\infty, +\infty]$ in the x-direction and $[0, \infty]$ in the y-direction. For the system in Fig. 1(b), the SC region is finite in the vertical y-direction and limited to the range of $[-L/2, +L/2]$. For this case, we will discuss the transmission probabilities after the SC region, therefore, the integration region will be taken as $[-\infty, +\infty]$ in the x-direction and $[+L/2, \infty]$ in the y-direction. Reflection (transmission) probabilities are obtained as the converged values of Eqs. (9) and (10), integrated only within the space before (after) the SC region, as $t \to \infty$.

The systems sketched in Fig. 1, where wave packets propagate from the bottom to the top, represent a setup where the bias is applied from the bottom to the top, along the vertical y-direction. In this case, the energy of the wave packet plays the role of potential bias in the actual experiment, whereas its width is related to e.g. a temperature broadening factor in Landauer-Buttiker formalism, as the wave packet width determines the range of energies/momenta of plane waves that are involved in composing the whole wave packet.[28]

III. RESULTS AND DISCUSSION

A. Uniform normal-SC interface in Dirac-Weyl materials: revisiting Andreev reflection in graphene

Let us first revisit the problem of Andreev reflection in graphene. Figure 1(a) shows a sketch of the proposed situation, where an electron in normal graphene propagates towards the superconducting region (shaded) through a trajectory that makes an angle α with the direction normal to the interface.

For the envelope function multiplying the pseudo-spin in Eq. (2), we assume a gaussian wave-packet

$$\psi(\vec{r},0) = \frac{1}{d\sqrt{2\pi}} \exp\left[-\frac{(x-x_0)^2 + (y-y_0)^2}{2d^2} + i\vec{k}_0 \cdot \vec{r}\right] \tag{11}$$

describing a propagating low energy electron in graphene. The band structure of Dirac-Weyl materials (e.g. graphene) around K and K' points of the first Brillouin zone can be approximated by linear functions that follow from diagonalization of the effective Hamiltonian

$$H_\pm = \hbar v_F(\pm k_x \sigma_x + k_y \sigma_y), \tag{12}$$

where v_F is the Fermi velocity and $\pm$ refers to K(+) and K'(-) cones, so that low energy electrons in this material behave as massless Dirac fermions. These cones are related by time-reversal symmetry, therefore, here we will consider only the case of electrons around K, whereas the behavior of electrons at K' are predicted from our results just by applying straighforward transformations due to the sign change in Eq. (12). This Hamiltonian enters Eq. (6) through the $\vec{\omega} = \vec{h}\Delta t/\hbar$ and $\vec{\omega'} = -\vec{h}\Delta t/\hbar$ terms, in this case, constructed by re-writting $H_\pm = (\pm h_x, h_y, 0) \cdot \vec{\sigma}$ with $\vec{h} = \hbar v_F \vec{k}$. The calculation is easily adapted e.g. for bilayer and trilayer graphene (in the ABC stacking order), using the 2×2 approximation for the Hamiltonian proposed in Ref. [29], where one just needs to re-define $\vec{h} = \frac{\hbar^2 v_F^2}{\gamma}(k_x^2 + k_y^2, \pm 2k_x k_y, 0)$ and $\vec{h} = \frac{\hbar^3 v_F^3}{\gamma^2}(k_x^3 - k_y^2 k_x, 3k_x^2 k_y - k_y^3, 0)$ for bilayer and trilayer cases, respectively, with γ as the inter-layer hopping parameter. While the results we will discuss further on here for mono and bilayer graphene revisit a topic that has been already theoretically studied,[3,4] although

somewhat less for the bilayer case, the results for trilayer graphene N/SC interfaces we will discuss in what follows are in fact rare in the literature. The calculations presented here could also be easily adapted e.g. for N/SC interfaces based on few layer black phosphorus, where low energy electrons are also described by a 2×2 Hamiltonian[30,31] that can be easily re-written in terms of the previously defined $\vec{h}$ vector.[32]

Notice that, for each of the different above mentioned materials, the most common approaches available in the literature to investigate transport through N/SC interfaces would require e.g. solving a whole new set of cumbersome differential equations and applying boundary conditions to match wave functions or currents at the interface between N and SC regions. This is one of the most important results of the present work: this problem is conveniently solved by the method developed here, where the wave packet propagation already accounts for the scattering at the interfaces in a numerical way, and no (semi-)analytical matching of wave functions or currents is explicitly required at the interfaces. Nevertheless, in order to do so, we pay the price of dealing with numerical Fourier transforms and finite size wave packets.[33]

The external potential is taken as $U(\vec{r}) \equiv 0$ and the superconducting gap $\Delta(\vec{r})$ is assumed to be a step functions that is zero for $y \leq 0$ and Δ_0 otherwise. We also assume a zero superconducting phase $\phi = 0$. From now onwards, we write energies in units of the SC gap Δ_0 and spatial coordinates in units of $r_0 = \hbar v_F/\Delta_0$. The wave-packet energy is fixed as $\varepsilon = 0.7\Delta_0$, which is used as input for Eq. (11) through the modulus of the wave vector, given by $k_0 = (\varepsilon + E_F)/\Delta_0 r_0$ in monolayer graphene. The wave-packet width is fixed as $d = 6.67 r_0$, which represents e.g. a $\Delta E \approx 0.15\Delta_0$ width in energy space for the monolayer case.

Figure 2 sketches the band diagrams in the normal (white) and superconducting (shaded) regions, for different values of Fermi level. When the Fermi level is much larger than the superconducting gap, $E_F \gg \Delta_0$, electrons with energy $\varepsilon < \Delta_0$ inciding in the superconducting region are reflected partially as holes. If the incidence is normal, the electron-hole conversion occurs with unit probability. On the other hand, if the trajectory of the incident electron makes a non-zero angle α with the vertical axis (see trajectories in Fig. 2 for $\alpha = 45^o$), a normal (electron) reflection is also expected. Moreover, the reflected hole is expected to propagate along the same trajectory as the incident electron, but with opposite propagation direction, which is known as Andreev retro-reflection. This is verified in the trajectory of electrons (blue symbols) and holes (red symbols) in Fig. 2(a), where darker (brighter) colors represent higher (lower) probability density. A small Goos-Hänchen shift is also observed between electron and hole trajectories.[34] The picture is however different if E_F is in the same order of magnitude as Δ_0, as in Fig. 2(b), where the almost no electron-hole conversion is observed. Furthermore, if $E_F \ll \Delta_0$, the converted hole wave function propagates

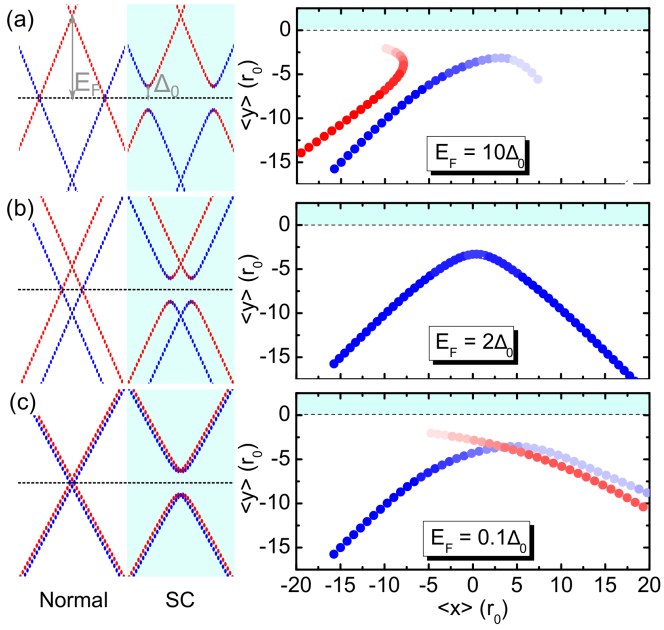

FIG. 2: (Color online) Sketch of the band structures in the normal and SC regions (left), and wave-packet trajectories (right), considering an incidence angle $\alpha = 45^o$ and three values of Fermi energy: (a) $E_F = 10\Delta_0$, (b) $E_F = 2\Delta_0$, and (a) $E_F = 0.1\Delta_0$. SC regions are highlighted as shaded areas in the figures. Color map in right panels is such that red (blue) represents hole (electron) wave-packets, whereas darker colors represent higher probability densities.

in the same direction as the reflected electron, as one verifies in 2(c), which is known as Andreev specular reflection.

Figures 3 and 4 illustrate Andreev retro- and specular reflections, respectivelly, by showing snapshots of the electron (blue) and hole (red) probability density distributions at three different instants in time. In the former (latter) the scattered electron and hole wave-packets clearly propagate towards opposite (the same) directions. Although it is not easy to experimentally observe snapshots of the wave packet propagation as those shown in Figs. 3 and 4, one can still track the trajectories and probability densities of electrons and holes along the system via scanning gate microscopy,[35] a technique that has been regarded as one of the most convenient tools to experimentally probe wave functions and transport properties in low dimensional systems, which has been recently successfully employed in the specific context of Andreev reflections in monolayer graphene-based N/SC interfaces in Ref. [9].

Considering momentum conservation along the x-direction of the system, one can infer the propagation direction of the Andreev reflected hole as follows: in the monolayer graphene case, the incident electron has a momentum $k_0 = (E_F + \varepsilon)/\hbar v_F$, while the Andreev scattered hole has momentum $k_h = (E_F - \varepsilon)/\hbar v_F$. Conservation of momentum along the horizontal direction requires $k_0 \sin\alpha = k_h \sin\alpha_h$, where α_h is the reflection angle of the

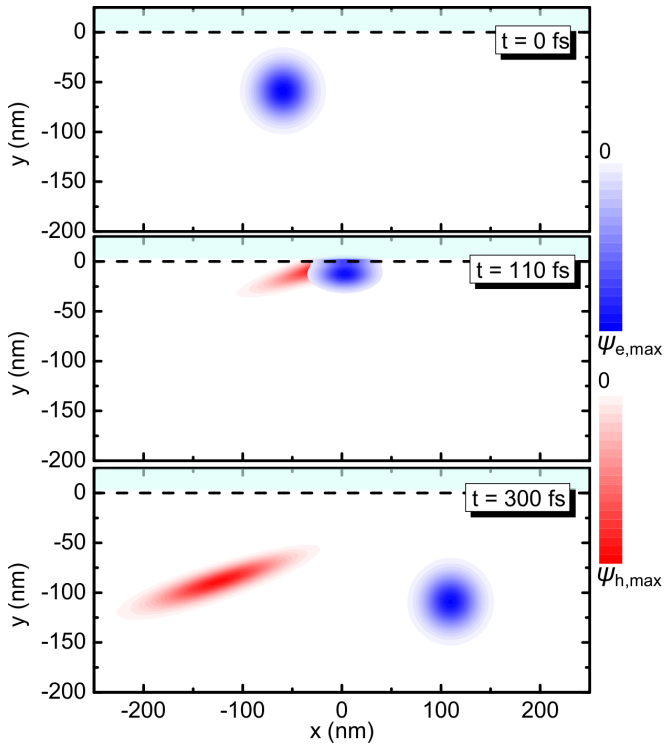

FIG. 3: (Color online) Snapshots of the wave-packet projections over the electron (blue) and hole (red) states, for a wave-packet in graphene being reflected by a superconduction region (shaded area) in $y > 0$, assuming $E_F = 10\Delta_0$. The snapshots are taken at three different instants in time, namely, $t = 0, 110$ fs and 300 fs.

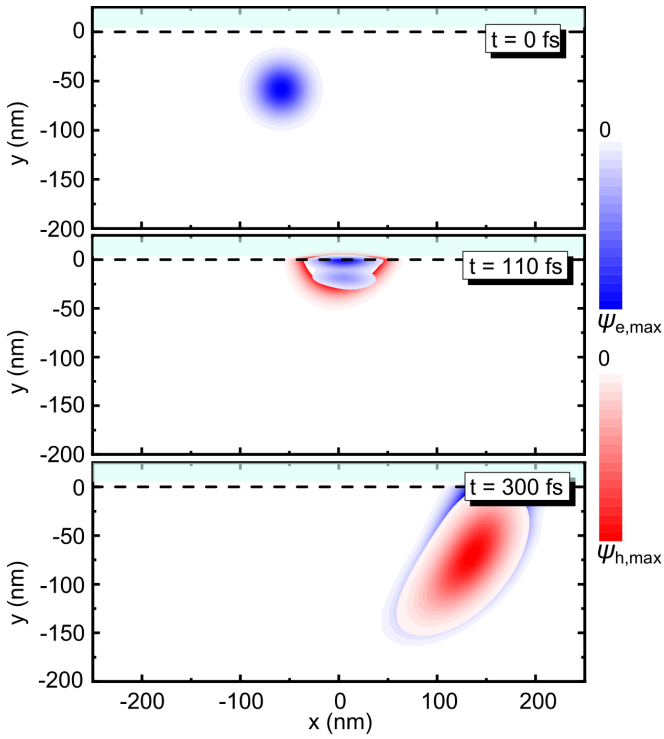

FIG. 4: (Color online) The same as Fig. 3, but for $E_F = 0.1\Delta_0$.

hole. This suggests the existence of a critical incidence angle beyond which the scattered hole propagates with $\alpha_h = \pi/2$. An interesting case happens when $\varepsilon = E_F$, where this critical incidence angle is zero and any hole that come from Andreev scattering has to propagate sideways along the x-axis, with zero momentum, regardless of the incidence angle α. This situation is illustrated in Fig. 5, which is similar to Fig. 4, but for an incident electron with energy $\varepsilon = 0.1\Delta_0 = E_F$. In the context of wave packets in monolayer graphene, a zero momentum hole wave packet would indeed exhibit a time evolution in the shape of a circular ring, see e.g. Refs. [36–38], just as the one observed in Fig. 5. It is clear that, while the reflected electron propagates backwards, the hole propagates sideways, which guarantees that holes cannot be collected in the region from which the electrons came in. A better visualization of this propagation is seen in the videos uploaded as Supplemental Material, for $\varepsilon = 7E_F$ and $\varepsilon = E_F$.[39] This effect is closely related to the basic concept behind the so-called crossed Andreev reflection (CAR), where a *pnp* junction is set up such that incoming electrons have the same energy as E_F, thus avoiding scattered holes in the source region, while the Fermi level in the drain region is set in a way that guarantees that only holes are collected there.[40–42] This suggests that, by properly tuning the potential and Fermi levels, one can conveniently use the method proposed here also in the study of CAR and co-tunneling phenomena in Dirac-Weyl materials. Moreover, by tracking the trajectories of refracted wave packets,[43] one can investigate the possibility of observing e.g. Veselago lens effect in such a *pnp* device,[44,45] which is left as an exciting perspective for future works.

Within the Blonder-Tinkham-Klapwijk (BTK) model, conductivity is proportional to $\int_0^{\pi/2}[1 - r(\varepsilon,\alpha) + r_A(\varepsilon,\alpha)]\cos\alpha d\alpha$, where r and r_A represent probabilities of observing a reflected electron and hole, respectively, after scattering of the incident electron by the SC interface. In graphene normal-SC interface, it is known that in the case of retro-(specular)reflection, i.e. for $E_F > \Delta_0 (E_F < \Delta_0)$, increasing the voltage V leads to an increase (decrease) in the conductivity.[3] It is not in the scopus of this paper to calculate the exact value of the conductivity. Nevertheless, one can use the method proposed here to verify this result. The integration kernel $I(\varepsilon,\alpha) = [1 - r(\varepsilon,\alpha) + r_A(\varepsilon,\alpha)]$ in the BTK expression is plotted as a function of the incidence angle in Fig. 6, assuming two values of Fermi level. Increasing the energy of the incident wave-packet, which plays the role of the voltage V in BTK model, leads to $I \times \alpha$ curves with consistently smaller area when $E_F > \Delta_0$, as in Fig. 6(a). Consequently, the integral of I with respect to the angle α decreases with ε, thus suggesting a conductivity that decreases with V. The opposite is true for $E_F < \Delta_0$, as in Fig. 6(b), where increasing the wave-packet energy

rather increases the area of the $I \times \alpha$ and, consequently, the conductivity.

As previously mentioned in Sec. III A, one advantage of the method proposed here is its flexibility to be easily adapted to other materials where charge carriers can also be described as Dirac-Weyl quasi-particles. As an example, we have calculated the time evolution and scattering of wave-packets in N/SC interfaces based on bilayer and trilayer graphene. Figures 7(a) and 7(b) show the integration kernel in the BTK model plotted as a function of the incident angle α, assuming two values of Fermi level, in the bilayer and trilayer cases, respectively.

For $E_F > \Delta_0$, the integrand I monotonically decreases with α in all cases, although with an area that is larger (smaller) for the trilayer (monolayer) graphene case, thus leading to higher (lower) conductivity. Notice that the results in Fig. 7 for $E_F > \Delta_0$ do not converge to 2 as $\alpha \to 0°$, as one would expect (see e.g. Fig. 6) e.g. from a plane wave calculation. This is due to the finite width of the wave packets considered here in the reciprocal space, which yields an energy distribution for the wave-packet that is significant in the case of $E_F > \Delta_0$. This issue is less relevant for monolayer graphene, where its linear energy dispersion ensures that the wave packet width in energy is proportional to its width in momentum. The energy dispersion in bilayer (trilayer) graphene, on the other hand, exhibits a second (third) order dependence on $\vec{k}$,[29] which yields wider distributions in energy for the wave packet, as compared to the monolayer case. As a consequence, bilayer and trilayer graphene cases require calculations with narrower momentum distributions, i.e. wider wave packets in real space, in order to keep the entire energy distribution of the wave packet below the superconducting gap. Indeed, we verified that increasing the wave-packet width (thus, narrowing down the energy distribution) leads to I at $\alpha = 0°$ consistently closer to 2. However, dealing with such wide wave-packets in a time propagation simulation makes the system computationally more demanding, due to the need for a much larger computational box, which makes the reproduction of Fig. 7 with large wave-packets prohibitive. Therefore, for the sake of consistency, we decided to keep these results in Fig. 7, assuming a wave-packet with the same width as in the other figures, and discuss them only in a qualitative way.

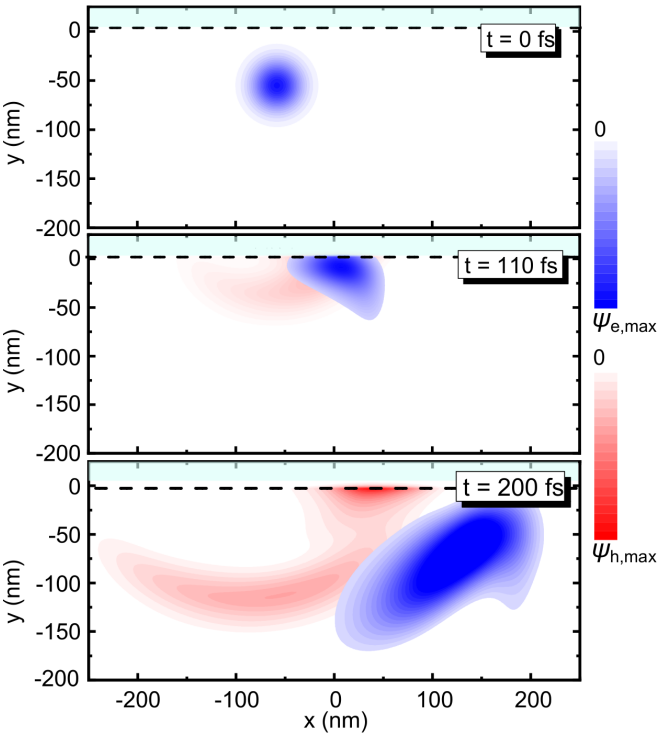

FIG. 5: (Color online) The same as Fig. 3, but for a wave packet with the same energy as the Fermi level, $\varepsilon = E_F = 0.1\Delta_0$.

Conversely, for $E_F < \Delta_0$, we observe that the value of the integrand I for $\alpha = 0°$ in the bilayer case is zero, which means that, at normal incidence, the electron is fully reflected by the barrier and no hole propagates through the normal region. This is in stark contrast with the results observed for both monolayer and trilayer graphene, where the integrand converges to 2 as $\alpha \to 0°$, and originates from the quadratic band structure of low energy electrons in bilayer graphene, which differs from that of mono and trilayer graphene cases. The integration kernel I in bi and trilayer graphene exhibit non-monotonic dependence on the incidence angle α, which also differs from the results observed for the monolayer case. The behaviour of the integrand I as a function of α observed in Figs. 6 and 7(a) are consistent with previous studies on monolayer[3] and bilayer[4], where this quantity has been calculated by matching quantum modes at the N/SC interface for some specific cases. This helps to validate the model proposed here, which, as previously mentioned, also allowed us to investigate trilayer graphene N/SC interfaces, a case that is not yet discussed in the literature in details, to the best of our knowledge.

B. Zero-gap channel in the superconducting region

In order to illustrate the versatility of the method proposed here for the study of N/SC interfaces with arbitrary shape and profile, we now investigate, as a sample case, the propagation of a wave front across a channel open in the SC region, as illustrated in Fig. 1(b), in monolayer graphene. The channel, which as a width W and a length L along the propagation direction, is tilted by 45° from the vertical axis, so that the first reflection by the normal-SC interface makes the electron propagate horizontally inside the channel.

The time evolution of P_e (blue) and P_h (red), integrated in the region after the SC ($[y_1, y_2] = [L/2, \infty]$ and $[x_1, x_2] = [-\infty, \infty]$, see Fig. 1(b)) is shown in Fig. 8, assuming $E_F = 10\Delta_0$ (solid) and $E_F = 0.1\Delta_0$ (dashed). In general, all P_e and P_h values are small, due to the fact

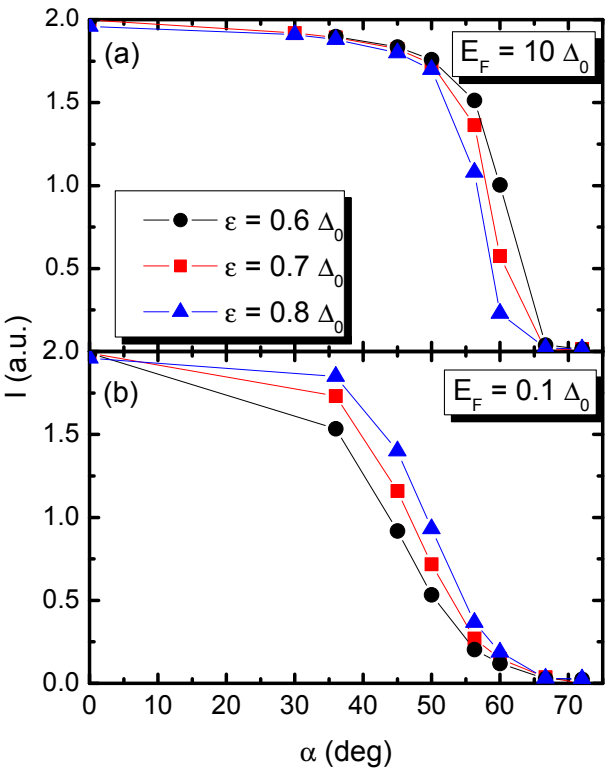

FIG. 6: (Color online) Integration kernel in the BTK model of conductivity as a function of the wave-packet incidence angle, assuming wave-packets with different energies ε and Fermi levels (a) $E_F = 10\Delta_0$ and (b) $E_F = 0.1\Delta_0$.

that most of the incoming electron wave front reaches the SC region aside of the channel entrance, and just a small fraction of it is actually capable of entering the channel region. The probability of finding an electron after the SC region is always non-zero, and it is higher for $E_F = 0.1\Delta_0$. However, the probability for holes to cross the channel is non-zero only for $E_F = 0.1\Delta_0$. Notice that in the absence of the channel, no hole is expected to be found after the SC region, regardless of the value of E_F, since for this value of incoming energy and potential landscape, we do not expect significant CAR. The trajectories of electrons (blue) and holes (red) illustrated in the insets help to understand the non-zero hole probability in the $E_F = 0.1\Delta_0$ case. As the electron is horizontally (vertically) reflected by the first (second) normal-SC interface in the channel, the resulting holes propagate in a direction that depends on E_F. For $E_F > \Delta_0$, the retro-reflected holes created in each normal-SC reflection propagate backwards along the same trajectory of the ongoing electron, thus, no hole is able to cross the channel. Conversely, for $E_F < \Delta_0$, specular-reflected holes arisen in each normal-SC reflection propagate along with the electron across the channel and eventually make their way through it, thus yielding non-zero hole probability beyond the channel.

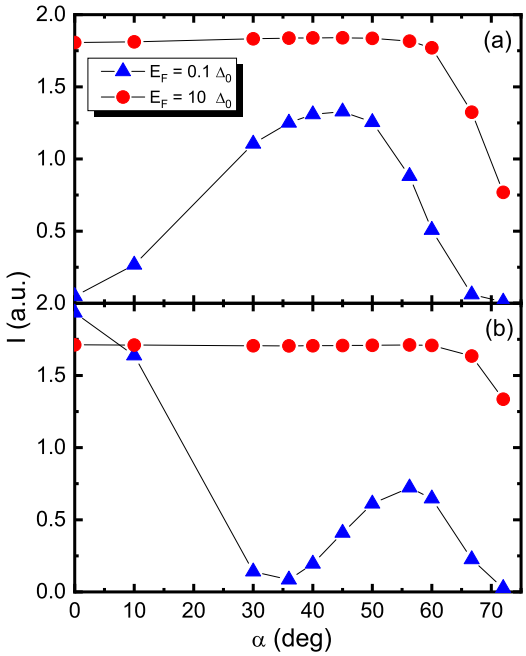

FIG. 7: (Color online) Integration kernel in the BTK model of conductivity as a function of the wave-packet incidence angle, assuming wave-packets with energy $\varepsilon = 0.7\Delta_0$ scattered by interfaces N/SC interfaces based on (a) bilayer (b) and trilayer graphene. Two values of Fermi level, $E_F = 0.1\Delta_0$ and $E_F = 10\Delta_0$, are considered.

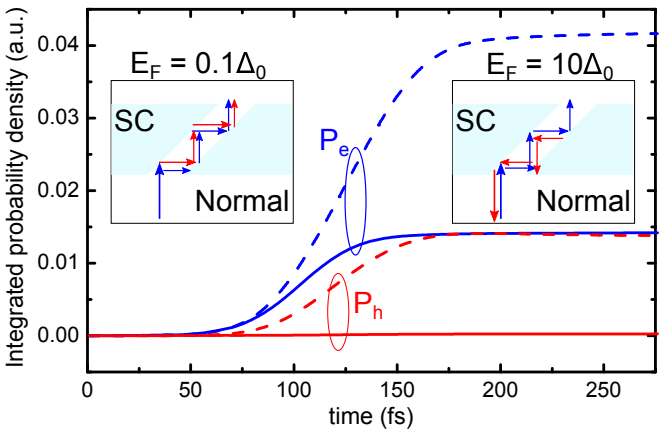

FIG. 8: (Color online) Electron (blue) and hole (red) integrated probability densities as a function of time in the normal region beyond a $W = 300$ Å, $L = 300$ Å channel in the superconducting region [see Fig. 1(b)], assuming Fermi energies $E_F = 10\Delta_0$ (solid) and $E_F = 0.1\Delta_0$ (dashed). Arrows in the insets illustrate the expected electron and hole trajectories undergoing reflections by the normal-SC interfaces.

The dependence of the electron and hole transmission probabilities on the width W and length L of the channel is shown in Figs. 9 and 10, respectively. For $E_F = 0.1\Delta_0$ and a fixed length $L = 300$ Å, results in Fig. 9(a) show that increasing the channel width W from 200 Å to 400 Å improves the hole transmission probability for wave-

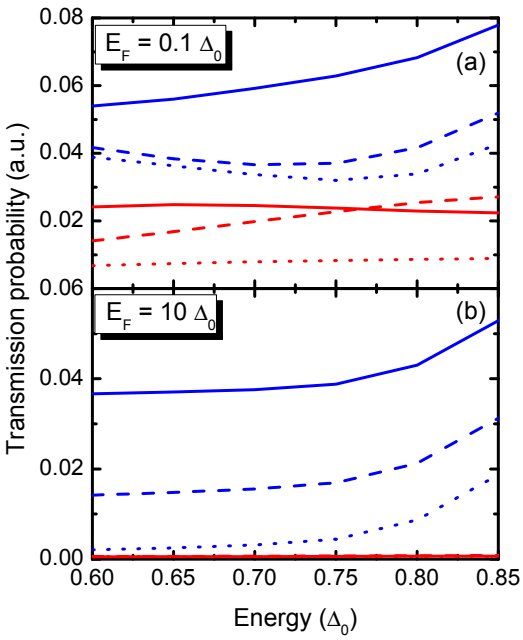

FIG. 9: (Color online) Electron (blue) and hole (red) integrated transmission probability as a function of the energy of the incoming wave front, assuming a channel in the superconducting region with length $L = 300$ Å, assuming widths $W = 200$ Å (dotted), 300 Å (dashed), and 400 Å (solid). Fermi energies are (a) $E_F = 0.1\Delta_0$ and (b) $E_F = 10\Delta_0$.

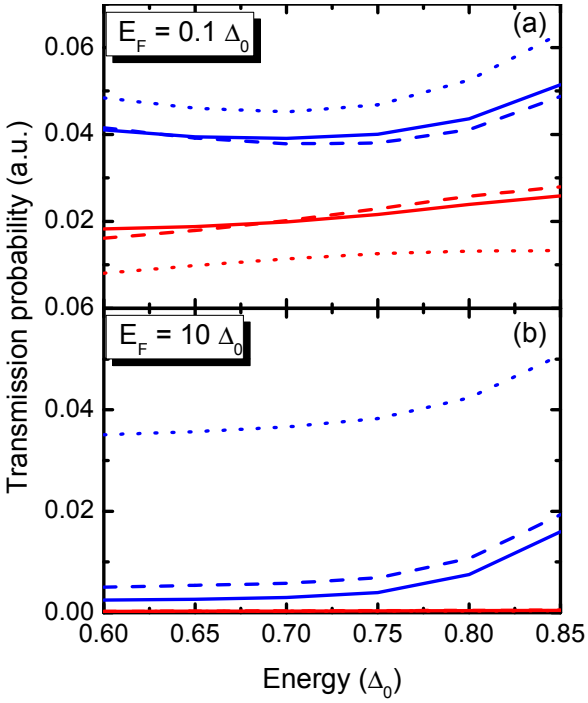

FIG. 10: (Color online) Electron (blue) and hole (red) integrated transmission probability as a function of the energy of the incoming wave front, assuming a channel in the superconducting region with width $W = 300$ Å, for lengths $L = 200$ Å (dotted), 350 Å (dashed), and 400 Å (solid). Fermi energies are (a) $E_F = 0.1\Delta_0$ and (b) $E_F = 10\Delta_0$.

packet energies lower than $\approx 0.775\Delta_0$. For higher energies, hole transmission probability for $W = 300$ Å is just slightly lower thant that for $W = 400$ Å. Nevertheless, a significant hole transmission probability is observed only for $E_F = 0.1\Delta_0$. For $E_F = 10\Delta_0$, Fig. 9(b) show an electron transmission probability that monotonically increase with the wave-packet energy, whereas hole probabilities are always vanishingly small. Qualitatively, this result persists for the whole energy range considered here, namely from $\varepsilon = 0.6\ \Delta_0$ to $\varepsilon = 0.85\ \Delta_0$. Similar conclusions are also drawn from the results in Fig. 10, where increasing the channel length L is demonstrated to yield equivalent results as decreasing the width W.

The 45° value was chosen for the angle of the tilted channel only for convenience, in order to facilitate the visualization of the results. One can easily verify that the same qualitative results would be observed for any angle. In fact, even a straight vertical channel shows a non-zero transmission probability for holes in the $E_F < \Delta_0$ case. However, this effect is much weaker for a vertical channel, since electron-hole conversion requires the wave function to bounce back and forth between the normal-SC interfaces in the channel, which is optimized as the angle between the channel and the vertical axis increase.

IV. CONCLUSIONS

In summary, we have proposed a general numerical technique to investigate electron scattering and electron-hole conversion at normal-SC interfaces with arbitrary shapes and profiles. The method, based on real time wave-packet propagation through a system described by a Bogoliubov-de Gennes model, is easily adapted for Dirac-Weyl-like Hamiltonians representing different two-dimensional materials, and allows one to observe electron and hole trajectories in a pedagogical and convenient way. As a sample case, we apply the method to revisit the problem of Andreev reflection in a normal-SC interface in monolayer graphene, where the transition from retro-reflection to specular reflection is observed just by tracking electron and hole trajectories as the Fermi level of the system is tuned. We then expanded this study to the investigation of Andreev reflection in bilayer and trilayer graphene cases as well, observing discrepancies with the monolayer graphene case, especially for wave-packets with energy lower than the superconducting gap. This illustrates how flexible the method proposed here is, being easily adapted to other Dirac-Weyl-like Hamiltonians.

As an example of an arbitrary profile of the SC region, we consider the case of an electron wave front propagating through a normal channel within the superconducting

region, tilted 45° with respect to the propagation trajectory of the incoming electron. The system is demonstrated to work as an electronic wave guide for any value of Fermi level E_F. However, the channel guides holes along with the electrons only for $E_F < \Delta_0$, whereas the retro-reflected holes in the $E_F > \Delta_0$ case propagate backwards and leave the channel via its entrance. This effect is enhanced as either the channel length or width are increased.

Exciting future prospects for this method are to investigate Andreev reflection in e.g. monolayer transition metal dichalcogenides and phosphorene, even under external applied electric and/or magnetic fields. Required modifications are straightforward, and therefore expected in imminent following studies. Results of these simulations are likely to be of interest to experimentalists working on heterostructures involving 2D materials and superconductors, as well.

Acknowledgments

This work was supported by the Brazilian Council for Research (CNPq), through the PRONEX/FUNCAP and PQ programs, and by the Flemish Research Foundation (FWO).

Appendix: time evolution of wave packets and pseudo-spins

The Suzuki-Trotter expansion[27] of the exponential in the time evolution operator in Eq. (3) yields

$$e^{-i\frac{H_{BdG}}{\hbar}\Delta t} = e^{-i\vec{W}_r\otimes\vec{\sigma}}e^{-i\vec{W}_k\otimes\vec{\sigma}}e^{-i\vec{W}_r\otimes\vec{\sigma}} + O(\Delta t^3) \quad (13)$$

where $\vec{W}_r = (\Delta_0\cos\phi, \Delta_0\sin\phi, U)\,\Delta t/2\hbar$, $\vec{W}_k = (0, 0, H - E_F)\frac{\Delta t}{\hbar}$, and the $O(\Delta t^3)$ error comes from the non-commutativity between $\vec{W}_r\cdot\vec{\sigma}$ and $\vec{W}_k\cdot\vec{\sigma}$ operators.

Since the exponential of arguments that depend linearly on Pauli vectors can be re-written as[24]

$$e^{-i\vec{S}\cdot\vec{\sigma}} = \begin{pmatrix} \cos(S) - i\sin(S)\frac{S_z}{S} & -i\sin(S)\frac{S_x - iS_y}{S} \\ -i\sin(S)\frac{S_x + iS_y}{S} & \cos(S) + i\sin(S)\frac{S_z}{S} \end{pmatrix}, \quad (14)$$

each of the exponentials in Eq. (13) are expanded in an exact way as matrices, which are eventually multiplied in sequence, as in Eq. (7).

---

* Electronic address: `andrey@fisica.ufc.br`

1. A. F. Andreev, Sov. Phys. JETP **19**, 1228 (1964).
2. A. H. Castro Neto, F. Guinea, N. M. R. Peres, K. S. Novoselov, and A. K. Geim, Rev. Mod. Phys. **81**, 109 (2009).
3. C. W. J. Beenakker, Phys. Rev. Lett. **97**, 067007 (2006).
4. T. Ludwig, Phys. Rev. B 75, 195322 (2007).
5. Yositake Takane, Katsuhide Yarimizu, Akinobu Kanda, J. Phys. Soc. Jpn. **86**, 064707 (2017).
6. D. K. Efetov , L. Wang, C. Handschin, K. B. Efetov, J.Shuang, R. Cava, T. Taniguchi, K. Watanabe, J. Hone, C.R. Dean and P. Kim, Nat. Phys. **12**, 328 (2016).
7. D. K. Efetov and K. B. Efetov, Phys. Rev. B **94**, 075403 (2016).
8. Abhiram Soori, Manas Ranjan Sahu, Anindya Das, Subroto Mukerjee, Phys. Rev. B **98**, 075301 (2018)
9. S. Bhandari, G.-H. Lee, K. Watanabe, T. Taniguchi, P. Kim, and R. M. Westervelt, Nano Lett. 20, 4890 (2020)
10. Gil-Ho Lee, Ko-Fan Huang, Dmitri K. Efetov, Di S. Wei, Sean Hart, Takashi Taniguchi, Kenji Watanabe, Amir Yacoby, and Philip Kim, Nat. Phys. **13**,693 (2017).
11. Chunxu Bai and Yanling Yang, J. Phys.: Condens. Matter **32**, 085302 (2020).
12. Yanling Yang, Bing Zhao, Ziyu Zhang, Chunxu Bai, Xiaoguang Xu, and Yong Jiang, Sci. Rep. **6**, 29279 (2016).
13. Tetsuro Habe, Phys. Rev. B **100**, 165431 (2019).
14. Xingfei Zhou, Phys. Rev. B **102**, 045132 (2020).
15. Han Liu, Adam T. Neal, Zhen Zhu, Zhe Luo, Xianfan Xu, David Tománek, and Peide D. Ye, ACS Nano **8**, 4033 (2014).
16. J. Linder and T. Yokoyama, Phys. Rev. B **95**, 144515 (2017).
17. A. Castellanos-Gomez, J. Phys. Chem. Lett. **6**, 4280 (2015).
18. S. Das, J. A. Robinson, M. Dubey, H. Terrones, and M. Terrones, Annual Review of Materials Research 45, 1 (2015)
19. Tony Low, Andrey Chaves, Joshua D. Caldwell, Anshuman Kumar, Nicholas X. Fang, Phaedon Avouris, Tony F. Heinz, Francisco Guinea, Luis Martin-Moreno, and Frank Koppens, Nature Materials **16**, 182 (2017).
20. A. Chaves, J. G. Azadani, Hussain Alsalman, D. R. da Costa, R. Frisenda, A. J. Chaves, Seung Hyun Song, Y. D. Kim, Daowei He, Jiadong Zhou, A. Castellanos-Gomez, F. M. Peeters, Zheng Liu, C. L. Hinkle, Sang-Hyun Oh, Peide D. Ye, S. J. Koester, Young Hee Lee, Ph. Avouris, Xinran Wang, and Tony Low, npj 2D Materials and Applications **4**, 29 (2020).
21. Arne Jacobs and Reiner Kümmel, Phys. Rev. B **64**, 104515 (2001).
22. Arne Jacobs and Reiner Kümmel, Phys. Rev. B **71**, 184504 (2005).
23. Gianluca Stefanucci, Enrico Perfetto, and Michele Cini, Phys. Rev. B **81**, 115446 (2010).
24. A. Chaves, G. A. Farias, F. M. Peeters, R. Ferreira, Communications in Computational Physics **17**, 850 (2015).
25. A. Chaves, V. N. Moura, F. J. A. Linard, L. Covaci, and M. V. Milošević, J. Appl. Phys. **128**, 124303 (2020).
26. P. G. De Gennes, *Superconductivity of Metals and Alloys* (Benjamin, New York, 1966).
27. M. Suzuki, Phys. Lett. A **146**, 319 (1990).
28. Tobias Kramer, Christoph Kreisbeck, and Viktor Krueckl, Physica Scripta **82**, 038101 (2010).
29. Edward McCann and Mikito Koshino, Rep. Prog. Phys.

76, 056503 (2013).

[30] Tony Low, A. S. Rodin, A. Carvalho, Yongjin Jiang, Han Wang, Fengnian Xia, and A. H. Castro Neto, Phys. Rev. B **90**, 075434 (2014).

[31] D. J. P. de Sousa, L. V. de Castro, D. R. da Costa, J. Milton Pereira, Jr., and Tony Low, Phys. Rev. B **96**, 155427 (2017).

[32] S. M. Cunha, D. R. da Costa, G. O. de Sousa, Andrey Chaves, J. Milton Pereira, Jr., and G. A. Farias, Phys. Rev. B **99**, 235424 (2019).

[33] Marcos H. Degani and Marcelo Z. Maialle, J. Comput. Theor. Nanosci. **7**, 454 (2010).

[34] C. W. J. Beenakker, R. A. Sepkhanov, A. R. Akhmerov, J. Tworzydło, Phys. Rev. Lett. **102**, 146804 (2009).

[35] H. Sellier, B. Hackens, M. G. Pala, F. Martins, S. Baltazar, X. Wallart, L. Desplanque, V Bayot, and S. Huant, Semiconductor Science and Technology **26**, 064008 (2011).

[36] Viktor Krueckl and Tobias Kramer, New J. Phys. **11**, 093010 (2009).

[37] I. R. Lavor, D. R. da Costa, Andrey Chaves, S. H. R. Sena, G. A. Farias, B. Van Duppen, and F. M. Peeters, J. Phy.: Cond. Matt. **33**, 095503 (2021).

[38] Andrey Chaves, L. Covaci, Kh. Yu. Rakhimov, G. A. Farias, and F. M. Peeters Phys. Rev. B **82**, 205430 (2010).

[39] Supplemental material containing videos of the propagation of wave packets with electron (top panels) and hole (bottom panels) components in a monolayer graphene N/SC interface at the $y = 0$ horizontal axis. Videos considering incoming electrons with energy $\varepsilon = 0.7\Delta_0 = 7E_F$ and $\varepsilon = 0.1\Delta_0 = E_F$, both at incidence angle $\alpha = \pi/4$, are provided.

[40] J. Cayssol, Phys. Rev. Lett. **100**, 147001 (2008).

[41] L. G. Herrmann, F. Portier, P. Roche, A. L. Yeyati, T. Kontos, and C. Strunk, Phys. Rev. Lett. **104**, 026801 (2010).

[42] S. Gómez, P. Burset, W. J. Herrera, A. L. Yeyati, Phys. Rev. B **85**, 115411 (2012).

[43] J. M. Pereira Jr, F. M. Peeters, A. Chaves, and G. A. Farias, Semicond. Sci. Technol. **25**, 033002 (2010).

[44] V. V. Cheianov, V. Fal'ko, and B. L. Altshuler, Science **315**, 1252 (2007).

[45] R. V. Gorbachev, A. S. Mayorov, A. K. Savchenko, D. W. Horsell, and F. Guinea, Nano Letters **8**, 1995 (2008).